PNAS RESEARCH ARTICLE | MEDICAL SCIENCES

Bioinspired nanogels as cell-free DNA trapping and scavenging organelles for rheumatoid arthritis treatment

Haofang Zhu[a,b], Bin Kong[a], Junyi Che[a], Yuanjin Zhao[a,c,1], and Lingyun Sun[a,b,1]

Edited by Natalie Artzi, Massachusetts Institute of Technology, Cambridge, MA; received March 1, 2023; accepted July 5, 2023 by Editorial Board Member Chad A. Mirkin

Excessive cell-free DNA (cfDNA) in the serum and synovium is considered a causative factor of rheumatoid arthritis (RA). Thus, cfDNA scavenging by using cationic polymers has been an effective therapeutic avenue, while these stratagems still suffer from systemic toxicity and unstable capture of cfDNA. Here, inspired by the biological charge-trapping effects and active degradation function of enzyme-containing organelles in vivo, we proposed a cationic peptide dendrimer nanogel with deoxyribonuclease I (DNase I) conjugation for the treatment of RA. Benefitting from their naturally derived peptide components, the resultant nanogels were highly biocompatible. More attractively, by tailoring them with a larger size and higher surface charge density, these cationic nanogels could achieve the fastest targeting capability, highest accumulation amounts, longer persistence time, and superior DNA scavenging capacity in inflamed joints. Based on these features, we have demonstrated that the organelle mimicking cationic nanogels could significantly down-regulate toll-like receptor (TLR)-9 signaling pathways and attenuate RA symptoms in collagen-induced arthritis mice. These results make the bioinspired DNase I conjugated cationic nanogels an ideal candidate for treating RA and other immune dysregulation diseases.

bioinspired | peptide dendrimer | nanogel | cell-free DNA | rheumatoid arthritis

Rheumatoid arthritis (RA) is an insidious autoimmune disease characterized by chronic inflammation and joint erosion (1, 2). Recent studies have revealed that the amounts of cell-free DNA (cfDNA) in the serum and articular cavity of RA patients are three orders of magnitude higher than that of healthy people (3–5). The cfDNA released from the damaged cells can stimulate toll-like receptor (TLR)-9 signaling pathways, which participate in the pathogenesis of RA (6, 7). Thus, cfDNA scavenging has been regarded as an effective therapeutic avenue of RA (8). In this aspect, driven by static charge interactions, cationic polymers can hamper the progression of joint inflammation in the RA model by neutralizing anionic cfDNA (9). However, the development of biocompatible cationic matters for RA treatment is still in its infancy (10, 11). Generally, most patients are refractory to the conventional intra-articular administration of these cationic drugs (12). In addition, the unstable electrostatic adsorption effects between the traditional cationic polymers and cfDNA may lead to incomplete eradication of cfDNA and further cause loss of therapeutic effects. Therefore, innovative and effective stratagems to locally and thoroughly scavenge cfDNA are still urgently anticipated.

Here, inspired by the biological charge-trapping effects and active degradation function of enzyme-containing organelles in vivo, we proposed a cationic peptide dendrimer nanogel with deoxyribonuclease I (DNase I) conjugation for the treatment of RA, as schemed in Fig. 1. Charge-trapping effects are ubiquitous in biology and influence various critical processes, including metabolism, protein degradation, cell signaling, and gene expression, by localizing charged functional molecules to specific domains (13–16). Thus, biostatic effects have been widely used in biomedicine, such as drug and gene delivery, bioluminescence imaging, and bioactive molecules capturing (17–22). In addition, organelles like mitochondria or lysosome serve as a comprehensive and versatile toolkit in vivo (23–26), contributing to the transformation of otherwise lethal chemicals to benign ones, even to nutrients (27, 28). To imitate the active function of organelles, various enzyme delivery vehicles have been successfully developed for targeting degradation of biological aggressors (19, 29–33). Therefore, it is conceivable that the employment of a nanocarrier with both charge-trapping ability and nuclease conjugation is expected to localize to inflamed joints, adsorb, decompose, and eradicate cfDNA, thereby radically alleviating the progression of rheumatoid diseases.

In this paper, by integrating DNase I into a third-generation polylysine dendrimer (G3K) nanogel, we developed a desired bioinspired nanocarrier as cfDNA trapping and scavenging organelles for RA treatment. As naturally derived peptide components, the

Significance

Excessive levels of cell-free DNA (cfDNA) in the serum and synovium have been identified as a causative factor of rheumatoid arthritis (RA). To address this issue, we have developed DNase I–conjugated cationic nanogels inspired by the biological charge-trapping effects and active degradation function of organellesas as cfDNA scavenger for RA management. Our organelle-inspired nanogels can effectively neutralize and eradicate the pathogenetic cfDNA, thereby blocking the downstream proinflammatory signaling pathways. Moreover, due to the naturally derived peptide components, the bioinspired cationic nanogels showed minimal toxicity in vitro and in vivo. Most importantly, when administered through an i.v. injection, the nanogels can quickly accumulate in RA joints in just 1 min, a feat that has never been achieved before.

Author contributions: Y.Z. and L.S. designed research; H.Z. performed research; B.K. and J.C. contributed new reagents/analytic tools; H.Z. and B.K. analyzed data; and H.Z. wrote the paper.

The authors declare no competing interest.

This article is a PNAS Direct Submission. N.A. is a guest editor invited by the Editorial Board.

[1]To whom correspondence may be addressed. Email: yjzhao@seu.edu.cn or lingyunsun@nju.edu.cn.

This article contains supporting information online at https://www.pnas.org/lookup/suppl/doi:10.1073/pnas.2303385120/-/DCSupplemental.

Published August 7, 2023.

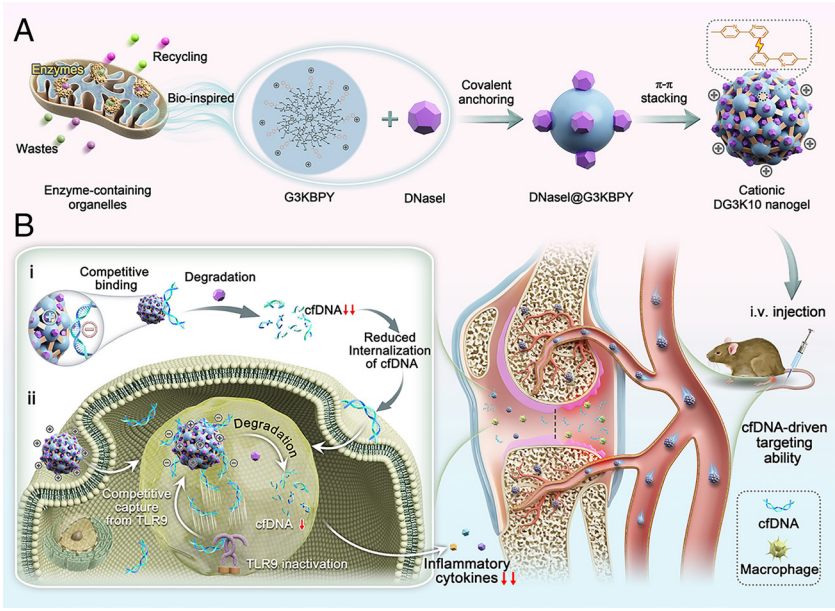

Fig. 1. Organelle-inspired cationic nanogels with DNase I conjugation inhibit RA development by locally binding and eradicating cfDNA. (*A*) Biomimetic construction of organelle-inspired cationic nanogels with DNase I decoration. (*B*) The cationic nanogels with cfDNA-driven targeting ability to inflamed joints effectively inhibit the TLR9 activation by i) intercellular and ii) intracellular neutralization of pathogenetic cfDNA.

resultant nanogels with varied structures and shell compositions all exhibited minimal toxicity in vitro and in vivo. More importantly, it was found that the nanogel with a larger size and higher charge density displayed the fastest targeting rate, highest accumulation amounts, and longest persistence time in inflamed joints. Based on the clinical scoring, paw swelling, microcomputed tomography (micro-CT) imaging, histological staining, and biochemical analysis, it was demonstrated that the nanogel could significantly attenuate RA symptoms, including ankle swelling and bone and cartilage damage. Notably, the cfDNA and proinflammatory cytokine levels in both inflamed joints and serum also corresponded with therapeutic outcomes. These distinctive features indicate that the bioinspired nanogel with DNase I conjugation may be promising candidates for the treatment of RA and shed light on nanomedicine in curing various autoimmune diseases.

Results

The cationic nanogels were prepared via aromatic interactions between the peripheral conjugated 2,2′-bipyridine-4-carboxylic acid (BPY) groups on third-generation lysine dendrimer (G3KBPY) (Fig. 2*A* and *SI Appendix*, Fig. S1). ^{1}H NMR spectrum (*SI Appendix*, Fig. S2) and Fourier transform infrared spectrum (FITR) (Fig. 2*B*) analyses were applied to characterize the chemical structure of G3KBPY. The unique chemical shift of unsaturated hydrogen atoms in ^{1}H NMR and the typical stretching vibration at 1,618 cm^{-1} of C=C in FITR validated the successful synthesis of G3KBPY. Besides, the blue shift of the BPY absorption peak from 290 nm in DMF to 230 nm in water revealed the cross-linking process of G3KBPY nanogel based on aromatic stacking between BPY groups (Fig. 2*C*). Since the shell composition determines the biological performance of nanogels, three molar ratios of G3K to BPY (1:2, 1:5, and 1:10) were used to optimize the synthesis of nanogels. Additionally, a lower

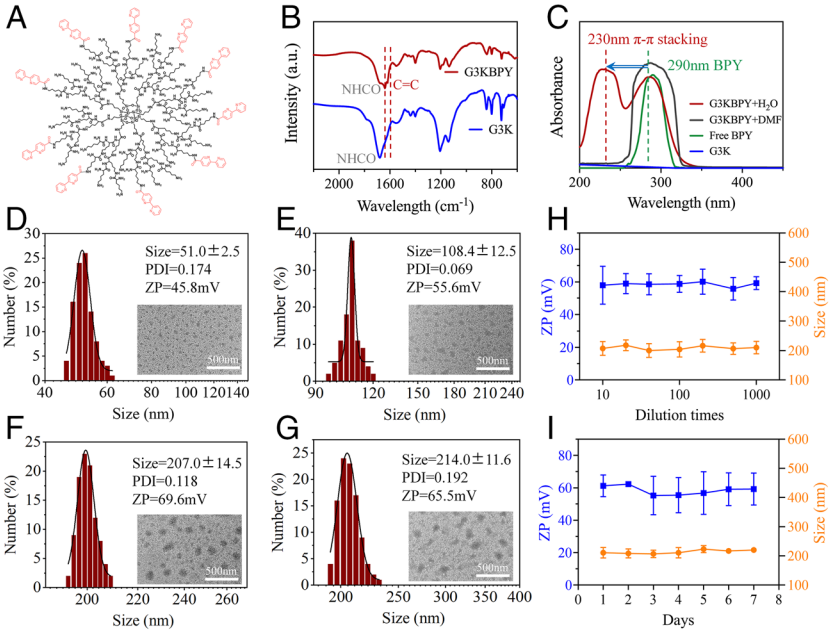

Fig. 2. The characterization of G3KBPY dendrimer and cationic nanogels. (*A*) Chemical structure of the G3KBPY dendrimer. (*B*) FITR spectra and (*C*) Ultraviolet (UV) spectra of G3K and G3KBPY dendrimers. (*D*–*G*) Hydrodynamic size distribution and TEM images of G3K2, G3K5, G3K10, and DG3K10 nanogels. Average particle size and zeta potential (ZP) of DG3K10 after (*H*) dilution with PBS and (*I*) reservation for 1 wk. Data are expressed as mean ± SD.

generation lysine dendrimer (G2K) modified with BPY (molar ratio of 1:10) was also applied as a control. The four resultant nanogels with different sizes and charge densities were defined as G3K2, G3K5, G3K10, and G2K10. Transmission electron microscope (TEM) scanning together with dynamic light scattering (DLS) analysis revealed the particle size and distribution (50 to 250 nm) and zeta potential (+25 to +70 mV) of nanogels with varied compositions (Fig. 2 *D*–*F* and *SI Appendix*, Fig. S3).

To ensure the thorough degradation of cfDNA following the ionic capture, we chemically conjugated nuclease (DNase I) onto the periphery of G3K10 to fabricate the DG3K10 nanogel. The nuclease conjugation content (CC) and nuclease conjugation efficiency (CE) on DG3K10 nanogel were determined by measuring the absorbance of fluorescent-labeled nuclease at 595 nm (*SI Appendix*, Fig. S4). DG3K10-2 was selected for subsequent studies because of its higher CC (15.4%) and CE (85.8%) (*SI Appendix*, Table S1). Besides, DLS and TEM analysis showed that the hydrodynamic size of DG3K10 (214 nm) was slightly larger than that of the G3K10 nanogels (Fig. 2*G*).

As intravenous (i.v.) injection may cause the disassembly of nanogels due to blood dilution, we therefore detected the stability of the nanogels against phosphate buffer saline (PBS) dilution and storage time (*SI Appendix*, Fig. S5). For all groups, the dilution led to constant zeta potential and a slight increase in particle size, suggesting minimal dissociation of the nanogels. Even after a 1-wk reservation, negligible changes were observed in both zeta potential and particle size. Notably, the decoration of DNase I did not affect the stability of the nanogel, as shown in Fig. 2 *H* and *I*, indicating the potentially better biochemical and biologic performance in vitro and in vivo.

Prior to the functional evaluation, the DG3K10 cationic nanogels were cocultured with mouse macrophages (RAW 264.7 cells) to determine the cytocompatibility by the cell-counting kit-8 (CCK-8) assay. We found that the DG3K10 cationic nanogels showed negligible cytotoxicity at all the tested concentrations (up to 500 μg/mL) (*SI Appendix*, Fig. S6), which could be attributed to their nature-derived peptide components and protein-like globular structure.

Based on their excellent biocompatibility in vitro, we next detected the DNA-binding efficiency (BE) of the cationic nanogels using an ethidium bromide (EtBr) competitive binding assay. G3K2, G3K5, G3K10, and DG3K10 nanogels showed a stronger trapping affinity than G2K10 in both PBS (pH 7.4) and fetal bovine serum (FBS, 10%) media, as the latter had a lower density of surface charges (Fig. 3*A*). This result indicated that the DNA scavenging ability of the cationic nanogels was not attenuated by the possible formation of protein corona around the nanogels once they entered the bloodstream via i.v. injection. It was noteworthy that the presence of serum did influence the DNA trapping efficiency of the nanogels when their mass ratio to DNA was lower than 1 (*SI Appendix*, Fig. S7). Additionally, to demonstrate the long-term activity of the nanogels, we measured their DNA-binding efficiency after storing them for 14 d at −20 °C. The results showed that the nanogels maintained high DNA-binding efficiency with only a

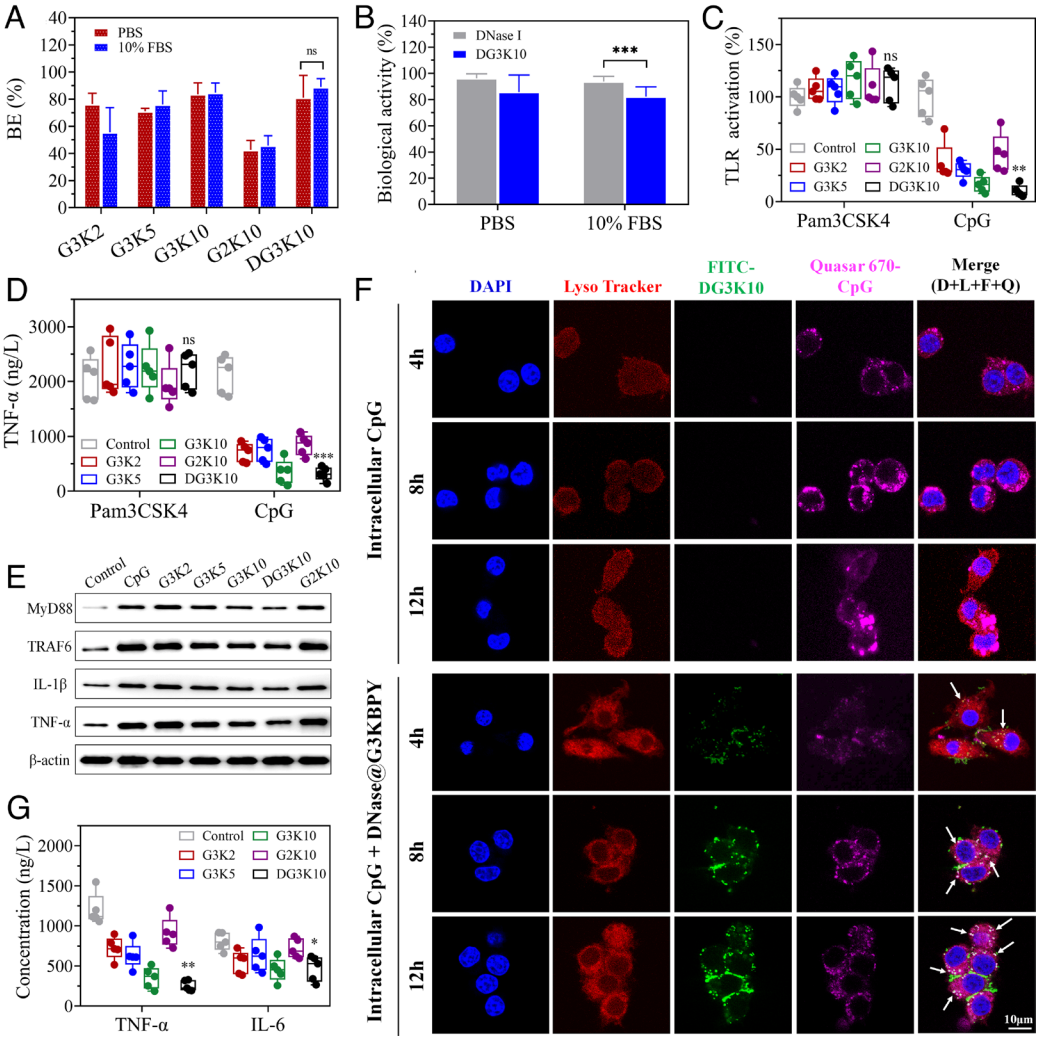

Fig. 3. Cationic nanogels inhibit cell inflammatory response due to a strong binding efficiency with extracellular and intracellular cfDNA. (*A*) EtBr competitive binding assay to measure the DNA binding efficiency of nanogels in PBS and in 10% FBS, respectively. The nanogels and DNA were mixed at a mass ratio of 1:1. (*B*) Biological activity of chemically anchored DNase I at pH 5 and 7.4, respectively. Cationic nanogels suppress NA-mediated activation of TLR9 in (*C*) Ramos BlueTM cells and (*D*) RAW264.7 cells. (*E*) MyD88, TRAF6, IL-β, and TNF-α enhanced expressions with CpG are down-regulated by cationic nanogels in Ramos BlueTM cells. (*F*) Intracellular trafficking of Quasar 670–labeled CpG and FITC-labeled cationic DG3K10 nanogels in RAW264.7 cells at different time points (Scale bar: 10 μm.) White spots marked by the white arrows indicate the colocalization of CpG and cationic nanogels. D: DAPI, L: LysoTracker, F: FITC-labeled DG3K10, and Q: Quasar 670-labeled CpG. (*G*) Cationic nanogels inhibit TNF-α and IL-6 expression of RA-FLS. RA-FLS was incubated with 1 μM of CpG 2006 for 4 h. Data are expressed as mean ± SD. $^{*}P < 0.05$, $^{**}P < 0.01$, $^{***}P < 0.001$ compared to the control group, using one-way ANOVA followed by a post hoc test.

slight decrease after 2 wk of storage (*SI Appendix*, Fig. S8). This could be attributed to their stable zeta potential and particle size in the aqueous solution (*SI Appendix*, Fig. S5 and Fig. 2 *H* and *I*).

Thorough clearance of cfDNA is expected to radically relieve RA symptoms and alleviate disease progression. Thus, the biological activity of DNase I anchored on nanogels at inflammatory joints is crucial. The in vitro biological activity of DNase I was studied at pH 7.4 (physiological condition) and pH 5 (inflammatory joints), respectively (34). Conjugated DNase I retained 88.54 to 89.17% of their original activities (compared with free DNase I) (Fig. 3*B*). This high biological activity of DG3K10 might be attributed to the "green" conjugation process based on active ester chemistry, which could maintain proteins' hydrogen bonds, reduce unfolding, and prevent protein deactivation (35).

We next examined whether the cationic nanogels with or without nuclease conjugation could inhibit cell inflammation activated by nucleic acid (NA)–based TLR agonist. While the cationic nanogel itself was unable to cause TLR activation in Ramos Blue™ reporter cells (*SI Appendix*, Fig. S9*A*), nanogels with varied sizes and surface charge densities (G3K2, G3K5, G3K10, G2K10, and DG3K10) all exhibited considerable suppressive capacities toward TLR9 activation by NA-based TLR agonist CpG-ODN2006 (Fig. 3*C*). Specifically, DG3K10 showed the strongest blocking efficiency in comparison with other nanogels, indicating that the better TLR inhibition resulted not only from the DNA-binding affinity but also from the DNA degradation capability of nanogel. Furthermore, all nanogels showed no response to a non-NA activator-medicated TLR stimulation (triacylated lipopeptide Pam3CSK4). Similar blocking capability was detected in RAW264.7 cells, in which all cationic nanogels could down-regulate the inflammatory cytokines and relieve the immune responses activated by CpG-ODN2006 but not Pam3CSK4 (Fig. 3*D*). It was noteworthy that none of the cationic nanogels alone could promote tumor necrosis factor-α (TNF-α) expression (*SI Appendix*, Fig. S9*B*), confirming our hypothesis that the specific NA-mediated TLR inhibition was achieved by the neutralizing effect between cationic nanogels with anionic NAs.

The result was further validated by western blotting analysis. CpG-ODN 2006 activated immune cells and induced proinflammatory cytokine production through the TLR–MyD88–NFκB signaling pathway. Once TLR9 sensed NAs, the adaptor molecule MyD88 was triggered, leading to the recruitment of TRAF6 and the activation of NFκB, which in turn caused severe autoimmune inflammation. As shown in Fig. 3*E*, both MyD88/TRAF6 protein expression in the downstream and RA inflammation related IL-1β/TNF-α proteins expression significantly decreased once CpG-ODN2006 was neutralized by G3K2, G3K5, G3K10, and DG3K10 nanogels. DG3K10 showed a superior down-regulating performance toward TLR activation due to its higher DNA-binding affinity and DNase I conjugation. We assumed that the cationic nanogels with a positive charge on their surface could bind and scavenge anionic cfDNA via electronic interaction, inhibit the intracellular trafficking of cfDNA from the plasma membrane to the endolysosomes, and prevent it from reaching the DNA sensors located on the endolysosomes, such as TLR9. By clearing cfDNA, the ligand for TLR9 is reduced, and therefore, the activation of TLR9 and its adaptor molecules MyD88 and TRAF6 is also reduced. This would lead to less phosphorylation and degradation of IκBα, which is an inhibitor of NFκB. As a result, NFκB would not translocate to the nucleus and induce the expression of inflammatory genes.

Then, we explored the probable cellular uptake-mediated mechanism of inflammation suppression. Quasar 670-labeled CpG-ODN2006 and FITC-labeled DG3K10 nanogels were coincubated with RAW264.7 cells for 12 h simultaneously. Their extra- and intracellular trafficking was observed by Confocal Laser Scanning Microscopy (CLSM) at 4, 8, and 12 h, respectively. The incorporation of DG3K10 did lead to a considerable reduction of internalized NAs (*SI Appendix*, Fig. S10), suggesting that cationic nanogels could recognize, scavenge, and further lower the internalization of extracellular inflammatory NAs.

In the above scenarios, cationic nanogels and CpG were added into cells at the same time. However, in actual situations, the pathogenetic cfDNA might already be internalized by immune cells when the therapeutics recognized them. To this end, we first incorporated CpG with the Ramos Blue™ reporter cells for 4 h. Then, the free extracellular CpG was thoroughly removed before the addition of DG3K10. At a dose of 250 μg/mL, DG3K10 showed a nearly complete inhibition in TLR9 activation. With a lower concentration at 100 μg/mL, TLR9 activation was down-regulated to 60%, implying the dose-dependent inhibitory manner of DG3K10 nanogels as TLR antagonists (*SI Appendix*, Fig. S11*A*). Similar anti-inflammatory behaviors were also observed in mouse macrophages (RAW264.7) (*SI Appendix*, Fig. S11*B*).

To further validate the competitive binding ability of cationic nanogels toward internalized cfDNA, we conducted an intracellular tracing study using Quasar 670-labeled CpG 2006 and FITC-labeled DG3K10 nanogels. The initial CpG uptake by endolysosome after 4 h incubation suggested the recognition of TLR9 (Fig. 3*F* and *SI Appendix*, Fig. S12). Then, CpG was removed, followed by the addition of DG3K10 cationic nanogels, and their intracellular colocalization was monitored in the next 12 h. Preferential enrichment of nanogels in the endolysosome compartment was observed, while the CpG intensity remained almost constant or even decreased. This specific intracellular capture of DG3K10 toward CpG may contribute to their superior in vivo therapeutic outcomes. Notably, the cationic nanogels could also inhibit the inflammatory response of fibroblast-like synoviocytes (FLS) from RA patients (Fig. 3*G*). In the presence of G3K2, G3K5, G3K10, and DG3K10 nanogels, the excess expression of proinflammatory cytokines, TNF-α and IL-6, was strongly suppressed. In contrast, the G2K10 nanogel with lower surface charge density showed minimal inhibition.

Although we have confirmed that the cationic nanogels could recognize and scavenge the pathogenetic cfDNA in vitro, their in vivo targeting efficiency remained unexplored. Thus, Alexa Flour 750-labeled nanogels were prepared, and their in vivo biodistribution in collagen-induced arthritis (CIA) mice by i.v. injection was studied using near-infrared fluorescence (NIRF) imaging. Fig. 4*A* showed the individual NIRF images for the first 2 h after DG3K10 injection. From these images, the cationic nanogels could be seen rapidly moving through the tail vein and immediately accumulating in the inflamed joints of CIA mice within the first few minutes. After 2 h, a strong NIR signal of AF750-labeled cationic nanogels was observed from the inflamed joints of CIA mice, whereas negligible fluorescence was detected in the joints of normal mice. Movie files depicting the path of DG3K10 post-injection into the tail vein of both CIA (Movie S1) and normal (Movie S2) mice are available.

It was also noted that all cationic materials showed distinctive joint-targeting efficiency in CIA mice while displaying minimal accumulation in normal mice, suggesting that the amounts of pathogenetic cfDNA did affect the biodistribution of cationic nanogels (*SI Appendix*, Fig. S13). NIR intensity of forepaws and hind paws treated with G3K10 or DG3K10 nanogels remained relatively strong even at 24 h posttreatment. CIA mice with G3K2,

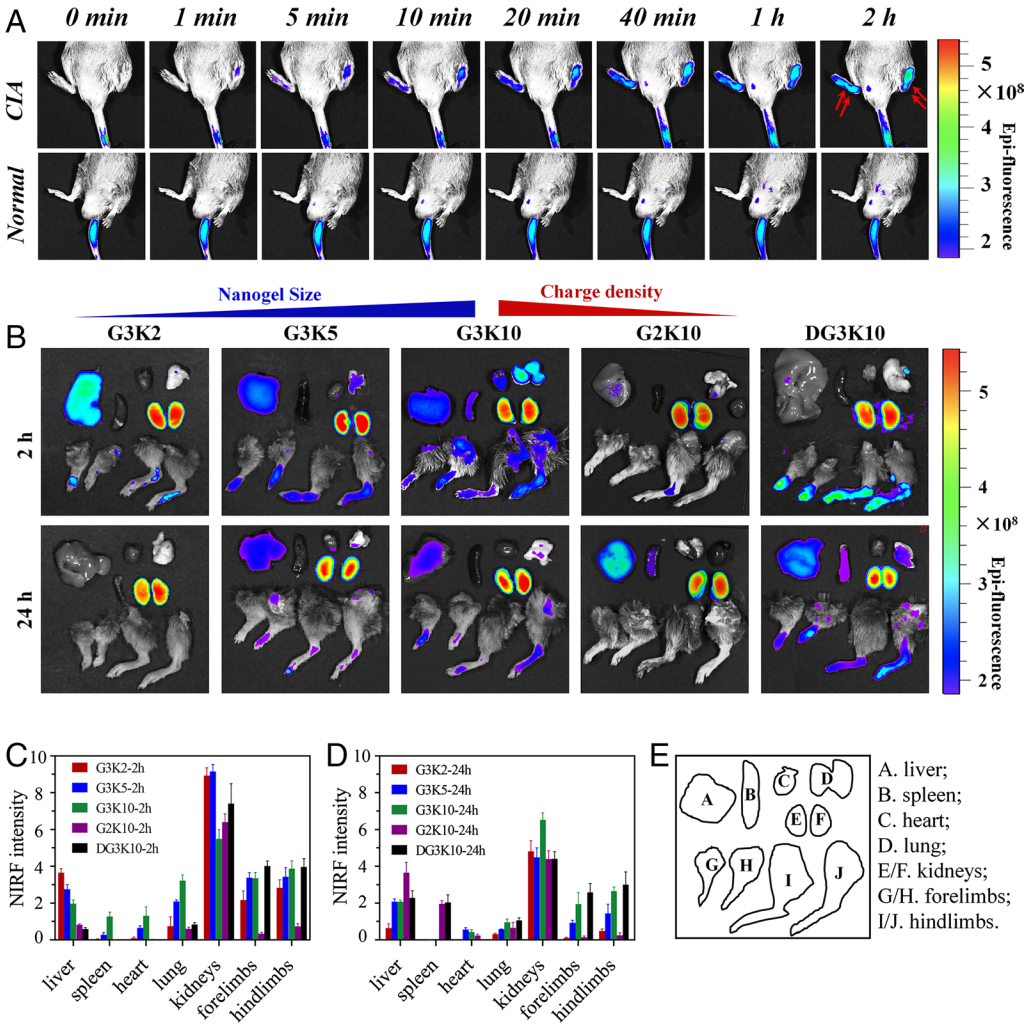

Fig. 4. The mechanistic studies of the favorable therapeutic performance of DG3K10 in treating RA. (*A*) Dynamic in vivo NIRF images of DG3K10 from 0 to 2 h. (*B*) The biodistribution of nanogels in extra-articular organs and joints at 2 h and 24 h postinjection by ex vivo NIRF imaging. Quantification of mean NIRF intensity of cationic nanogels in ex vivo biodistribution study of CIA mice at (*C*) 2 h and (*D*) 24 h after i.v. injection. (*E*) A). liver; B). spleen; C). heart; D). lung; E/F). kidneys; G/H). forelimbs; I/J). hindlimbs. Data are expressed as mean ± SD.

G3K5, and G2K10 treatment showed a noticeable reduction in NIR signal and were barely detectable after 24 h, suggesting that both the targeting efficiency and joint retention time increased with higher charge density and larger size of nanogels.

We also measured the biodistribution of nanogels in extra-articular organs and joints (Fig. 4*E*). At 2 h postinjection, much more G3K10 and DG3K10 nanogels accumulated in the joints of CIA mice compared with G2K10, correspondingly showed a lower NIR signal in internal organs (Fig. 4 *B* and *C*). We assumed that the higher surface charge density was an essential prerequisite for specific targeting of nanogels to inflamed joints. After 24 h, G3K10 and DG3K10 nanogels still showed considerable accumulation in the joints and paws, reinforcing the conclusion that larger size distribution and higher charge density efficiently prolonged the joint retention time of nanogels (Fig. 4*D*). In contrast, nanogels with smaller size tended to accumulate in the lung, liver, and kidney rather than joints and paws. However, the NIR signal in the kidney of the DG3K10 group showed a significant increase with the prolongation of time as the DG3K10 was partially degraded into small pieces. These analyses validated that the nanogels with higher surface charge density and larger size preferred clustering in the inflamed joints and showed longer retention time. This targeting behavior of cationic nanogels might be attributed to the small vascular leakage of pannus and the high local anionic cfDNA accumulation in rheumatoid joints.

In an animal model, one day after injection of 10 μg CpG into the articular cavity, all rats have already developed arthritis with typical features of severe erythema and striking hyperthermia in joints. The animals were then treated with i.v. injection of cationic nanogels at a daily dose of 25 mg/kg for the following 7 d (Fig. 5*A*). As a positive control, an i.v. injection of methotrexate (MTX), which was the first-line drug and the gold standard used to treat RA, was administered. The DG3K10 treatment outperformed the others in reducing the swelling in the hind paws (Fig. 5*B* and *SI Appendix*, Fig. S14*A*). Paw temperature associated with inflammation was also relieved to varying degrees observed by thermography (TG) (Fig. 5*c*). By day 8, the swelling and temperature of the hind paws treated by DG3K10 had almost returned to normal. On the contrary, swollen ankle and hyperthermia were still visible in MTX-, G3K5-, and G2K10-treated groups.

The microcomputed tomography (micro-CT) images showed that bone destruction, as highlighted by the yellow arrows, was undetectable after the treatment of DG3K10 for 7 d. Bone mineral density (BMD), a typical marker for the bone loss of arthritis joints, of the DG3K10-treated group recovered from 1,181 to 1,780 mg/cm^3, a level close to that of the normal rats (Fig. 5 *D* and *E*). In addition to bone erosion, synovitis is another common RA symptom. We stained ankle joints with H&E, toluidine blue (TB), and safranin O (SO) after 7 d of different treatments to assess inflammation and soft tissue disorder. After treatment with DG3K10 nanogels, the pathological analysis revealed a huge drop in inflammatory cell infiltration and a much clearer cartilage boundary, similar to those of the healthy group. (*SI Appendix*, Fig. S14 *B* and

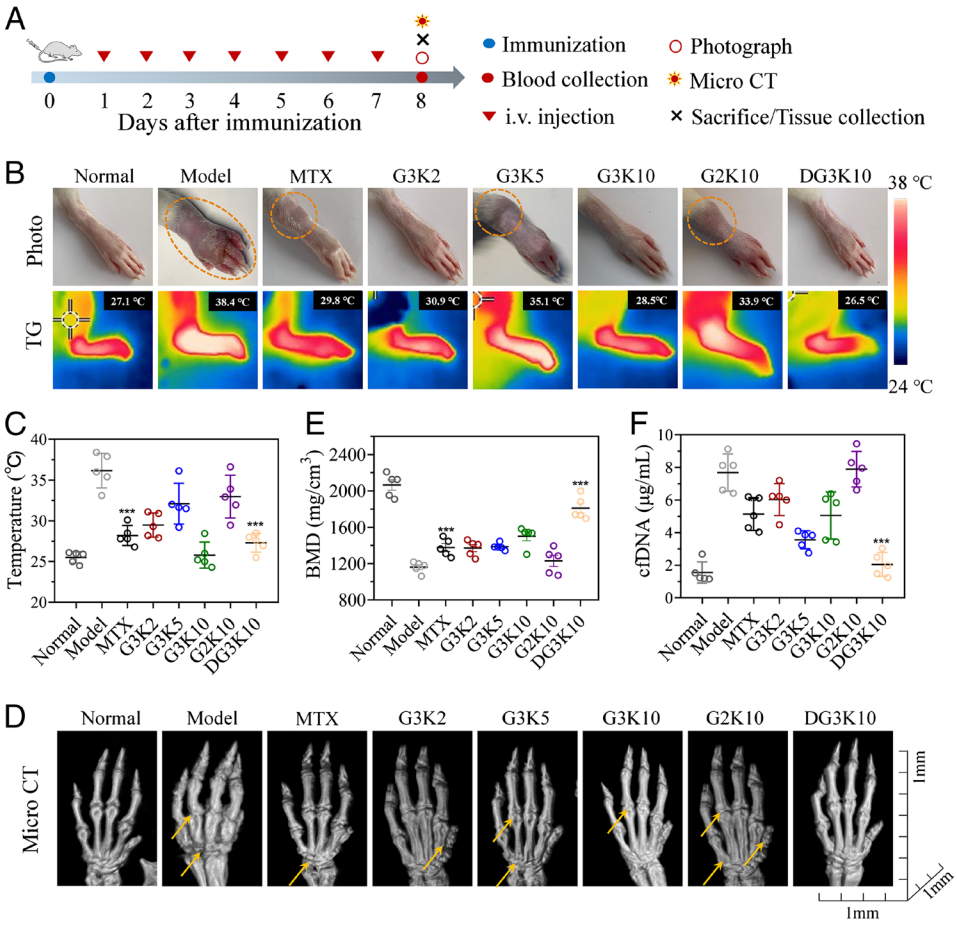

Fig. 5. DG3K10 nanogels improve the arthritic condition of SD rats induced by CpG. (*A*) Schematic representation of the establishment and treatment of the CpG-induced rat RA model. (*B*) Photos and thermographic (TG) images of right hind paws after administration of 7 d. The circled region indicated the swollen popliteal lymph node. (*C*) Quantification of paw temperatures at day 8. (*D*) The RA repairment of ankle joints was monitored by micro-CT images. Yellow arrows indicated the bone erosion. (*E*) The BMD of ankle joints were calculated from the micro-CT reconstruction. (*F*) Serum cfDNA concentration in RA rats after the treatment of nanogels and MTX for 7 d. Data are expressed as mean ± SD. ***P < 0.001 compared to the control group, using one-way ANOVA followed by a post hoc test.

C). Overall, the beneficial therapeutic effects of DG3K10 in CpG-induced RA models were due to its cfDNA-driven homing ability and the better cfDNA clearance ability in systemic circulation (Fig. 5*f*).

We next evaluated the in vivo therapeutic performance of DG3K10 nanogel using a mouse CIA model with similar pathological presentations resembling human RA. Following the onset of CIA at day 42, cationic nanogels were i.v. administered at a dose of 25 mg/kg of body weight weekly for 4 wk (Fig. 6*A*). Beyond day 49, all cationic nanogels showed reduced swelling and erythema in hind paws. It was noted that the DG3K10 group loaded with DNase I outperformed its counterparts without nuclease conjugation (G2K10, G3K2, G3K5, and G3K10) and the conventional MTX (Fig. 6*B* and *SI Appendix*, Fig. S15). With the treatment of DG3K10, hind paws swelling decreased to a nearly normal level at day 70. Moreover, both hind paws and forepaws of DG3K10-treated mice showed significantly improved clinical scores, demonstrating the positive therapeutic effects of nuclease-loaded cationic nanogels (Fig. 6*C* and *SI Appendix*, Fig. S16). Notably, DG3K10 nanogels showed higher efficiency in the capture and disintegration of cfDNA in the systemic circulation (Fig. 6*D*), which was possibly aided by their DNase-I conjugation and longer retention time in vivo. In contrast, MTX, G3K2, G3K5, G3K10, and G2K10 treatment without nuclease showed minimal reduction in the systemic cfDNA level.

The bone erosion in CIA mice was monitored by micro-CT imaging (Fig. 6*I*). Varying levels of bone destruction in the ankle (*SI Appendix*, Fig. S17*A*), knee (Fig. 6*F*), and wrist (*SI Appendix*, Fig. S17*B*) joints were observed for all treatment groups. BMD was calculated by micro-CT reconstruction. At day 29, the CIA model group showed a significant decrease in BMD for ankle (*SI Appendix*, Fig. S17*C*), knee (*SI Appendix*, Fig. S17*D*), and wrist (*SI Appendix*, Fig. S17*E*) joints, indicating serious bone destruction. Treatment with MTX, G3K2, G3K5, G3K10, and G2K10 resulted in a slight improvement of BMD between days 42 and 70. In contrast, DG3K10 nanogels group demonstrated normal BMD levels, implying evident inhibition of erosive bone damage.

H&E, toluidine blue, safranin O, and tartrate-resistant acid phosphatase (TRAP) staining of the RA joints suggested severe bone and synovium destruction accompanied by decreased chondrocytes and intense leukocyte invasion (Fig. 7 and *SI Appendix*, Fig. S18). Compared with control and model groups, the DG3K10-treated mice showed considerable restoration of soft tissues and significant reduction of histology scores (Fig. 7*A* and *SI Appendix*, Fig. S19*A*), verifying the efficient therapeutic outcomes of cationic DG3K10 nanogels. Glycosaminoglycans in cartilage stained with toluidine blue and safranin O showed an apparent cartilage loss in the model group, suggesting severe joint damage (*SI Appendix*, Fig. S19 *B* and *C*). The number of cells that stained positive for TRAP, which is indicative of osteoclasts, decreased with the treatment of DG3K10 nanogels. Interestingly, thanks to the efficient capture and degradation of cfDNA driven by cationic nanogels, the DG3K10 group exhibited a nearly normal synovial boundary comparable to those of the healthy group. This indicated the potential cartilage protective effect of the DG3K10 for RA treatment.

We also conducted the immunofluorescent staining of paw joints (Fig. 7*B*). Key diagnostic biomarkers related to the pattern recognition receptor (PRR) signaling pathways of RA, including TNF-α, IL-6, and collagen degradation associated matrix metalloproteinase (MMP)-3/13 in synovial fluid were measured. Notably, DG3K10 treatment brought the expression of inflammatory cytokines and

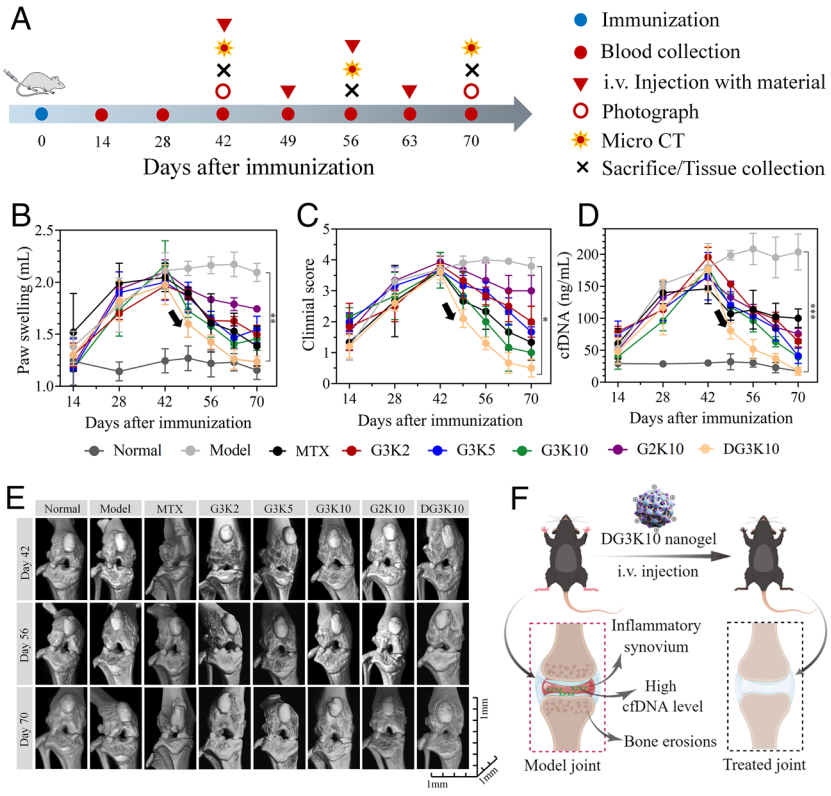

Fig. 6. In vivo therapeutic effects of cationic nanogels in the CIA model. (*A*) Schematic representation of the establishment and treatment of the CIA mice model. (*B*) Hind paw swelling, clinical scoring of (*C*) hind paws of CIA mice in the process of establishment and treatment by cationic nanogels. (*D*) Serum cfDNA concentration in CIA mice with the treatment of nanogels at different time points. (*E*) The RA progression and repairment of knee joints were monitored by micro-CT images. (*F*) Illustration of RA joint destruction and regeneration. Data are expressed as mean ± SD. $^{*}P < 0.05$, $^{**}P < 0.01$, $^{***}P < 0.001$, using one-way ANOVA followed by a post hoc test.

MMP-3/13 down to a normal level, consistent with the lower cfDNA levels in the synovial joints (*SI Appendix*, Figs. S20–S22). The MTX, G3K2, G3K5, G3K10, and G2K10 treated groups could only show a certain degree of reduction in inflammation and collagen degradation. The results were further confirmed by the mRNA expression and the systemic cytokines levels (*SI Appendix*, Figs. S23 and S24). We found that DG3K10 treatment restored TNF-a, IL-6, and MMP-3/13 expression to levels comparable to normal mice, implying a more effective inhibition of RA.

To obtain insight into the mechanism for DG3K10 treatment, we performed mRNA sequencing (RNA-seq) on the synovial tissue of CIA mice. Compared to the model group, the DG3K10 group showed a differential upregulation of 2,600 genes and down-regulated 2,331 genes [$P < 0.05$, $|\log2(\text{fold change})| > 1$] (Fig. 8*A*). Gene ontology (GO) enrichment analysis showed that the therapeutic effects of DG3K10 on RA mice were associated with the "TLR signaling pathway" and "activation of innate immune response" in biological processes (BP), "endocytic vesicle" and "endosome membrane" in cellular components (CC), and "TLR binding" and

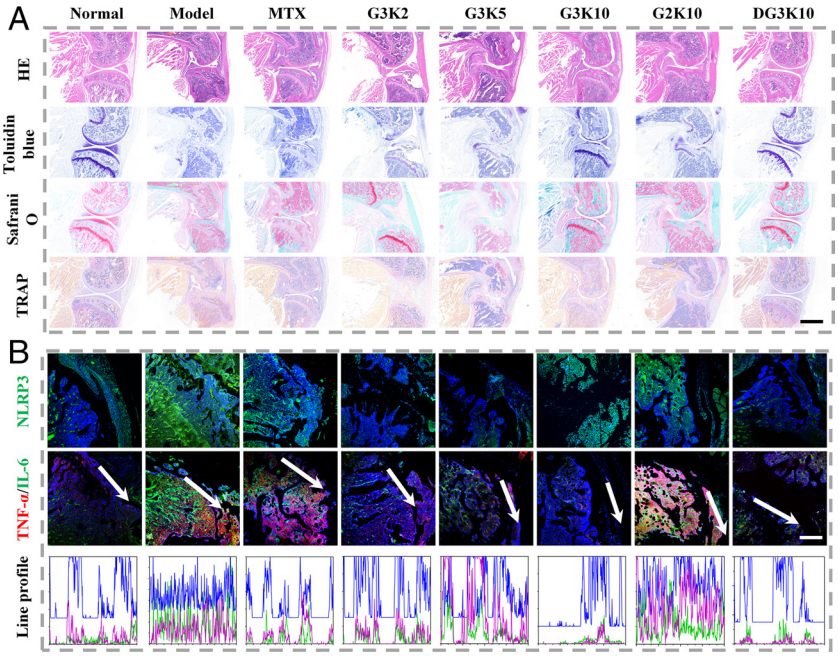

Fig. 7. In vivo histology outcomes with the treatment of cationic nanogels in the CIA model. (*A*) H&E, toluidine blue, safranin O, and TRAP staining, and (*B*) NLRP-3, TNF-α, and IL-6 immunofluorescent staining of the knee joint of CIA mice at day 70 after immunization. Coexpression and colocalization of TNF-α and IL-6 were confirmed by line profile analysis. (Scale bar, 200 μm.)

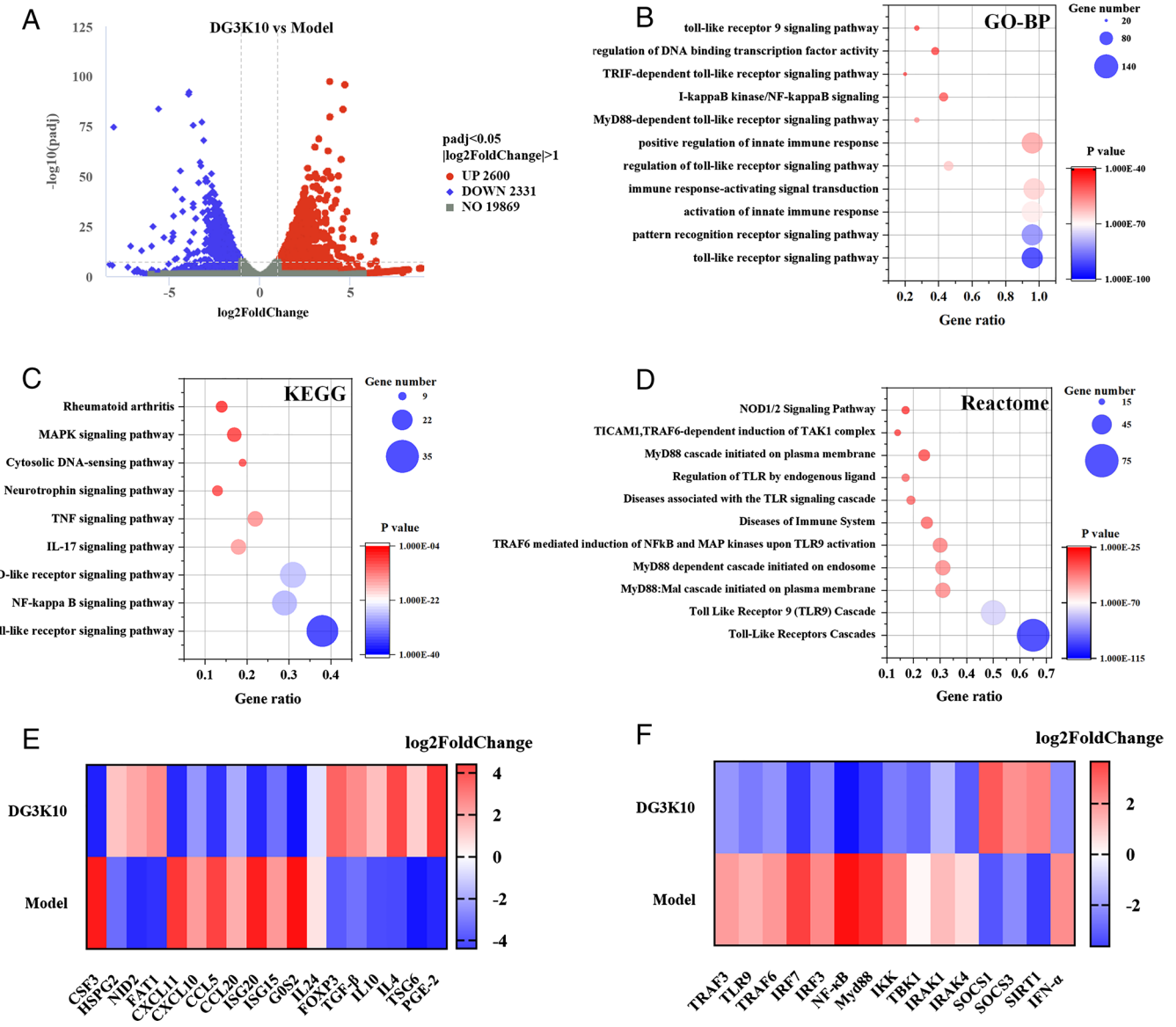

Fig. 8. Therapeutic mechanisms of DG3K10 nanogels in the CIA model. (*A*) Volcano plot of differentially expressed genes between DG3K10-treated and model groups. (*B*) GO, (*C*) KEGG, and (*D*) Reactome enrichment analyses of differentially expressed genes in the DG3K10-treated and model group. Enrichment analyses were performed using Database for Annotation Visualization and Integrated Discovery (DAVID) Bioinformatics. BP, biological processes; CC, cellular components; MF, molecular functions. (*E*) Heat map of the immune regulation-related genes. (*F*) Heat map of the TLR signaling transduction-related genes.

"sequence-specific DNA binding transcription factor recruiting" in molecular functions (MF) (Fig. 8*B* and *SI Appendix*, Fig. S25). Pathway enrichment analysis using Kyoto Encyclopedia of Genes and Genomes (KEGG) and Reactome showed that DG3K10 nanogels modulated pathways related to the TLR-9 signaling pathway, MyD88-TRAF6-NFκB-dependent cascade, cytosolic DNA-sensing pathways, and key cytokines like tumor necrosis factor (Fig. 8 *E* and *F*). Heat map analysis indicated that DG3K10 treatment up-regulated genes involved in immune regulation and down-regulated genes involved in TLR9 activation and inflammatory cytokine production (Fig. 8 *G* and *H*). Collectively, these results suggested that DG3K10 nanogels exerted anti-inflammatory effects by interfering with key molecular pathways involved in RA pathogenesis.

Poor in vivo biocompatibility can severely hinder the clinical translation prospect of biomaterials. DG3K10 showed a favorable therapeutic performance to ameliorate RA progression and displayed minimal toxicities with a mice death rate of 0% throughout the treatment (*SI Appendix*, Fig. S26). Histological analysis of the major organs was conducted to further analyze the systemic biocompatibility of cationic nanogels. The results showed that all cationic nanogels based on the peptide dendrimer showed negligible organ lesions (*SI Appendix*, Fig. S27), suggesting their superior long-term biocompatibility, which was consistent with in vitro studies. Besides, the hepatotoxicity in CIA mice treated with peptide dendrimer nanogels as reflected in alanine aminotransferase (ALT), alkaline phosphatase (ALP), and aspartate aminotransferase (AST) and, additionally, nephrotoxicity as reflected in creatinine, uric acid, and urea levels were comparable to that in normal mice (*SI Appendix*, Fig. S28). The favorable biocompatibility of cationic nanogels may contribute to their naturally derived peptide components and specific inflamed joints targeting biodistribution profile, allowing for local scavenging of cfDNA to relieve RA progression without systemic side effects.

Discussion

In this work, inspired by the biological charge-trapping effects and active degradation function of organelles, we have developed a DNase

I–conjugated cationic nanogel as a cfDNA scavenger for RA management. The surface decoration of DNase I makes it possible for the cationic nanogels to not only neutralize the pathogenetic cfDNA but also break it down into small pieces. This completely blocks the downstream proinflammatory signaling pathways. Previous research on cfDNA, on the other hand, focused only on ionic capture but not disintegration (3, 4, 8, 9, 36, 37). Due to the naturally derived peptide components, the bioinspired cationic nanogels showed minimal toxicity in vitro and in vivo. This resolves the issue with conventional cationic polymers used for cfDNA capture, in which stronger binding affinity is also accompanied by a marked increase in toxicity. Most importantly, by giving the nanogels through an i.v. injection, they could quickly accumulate in RA joints in just 1 min. This would speed up the move toward precision medicine in RA treatment.

Although the nanoparticle system imitating the biological process has distinct benefits, several aspects still need further refinement. First, for the design of the nanogels, the incorporation of an intelligent outer shell with both stealth effect on the host immune system and specific targeting ability to the lesion area is recommended. Since the "don't eat me" and "homing" signals will minimize the immune clearance and systematic side effects. Second, enzyme-immobilized cationic nanogels require further decoration of functional groups to simulate the working environments of biological enzymes and to achieve high enzyme activity for cascade reactions. Third, to realize the complex and bionic recycling processes in the body, we need to study more biological interactions and enzymatic processes and integrate them into the system. Regarding future clinical translation of the nanogels, it is critical to consider scale-up and manufacturing issues because of the use of synthetic polylysine dendrimers. Microfluidic technology offers a platform for chemical synthesis toward either molecules or nanomaterials, which has promoted the progress of biomedicine and enabled the supply of the peptide dendrimer for clinical studies (38–40). These efforts together offer a promising prospect for the translation of smart nanogels and a comprehensive biomimicking strategy in general.

Materials and Methods

Synthesis and Characterization of G3KBPY. To prepare G3KBPY, polyhedral oligomeric silsesquioxane (POSS) core-based G3K was synthesized. Detailed descriptions of the procedure have been included in *SI Appendix, Materials and Methods*.

Fluorescent Labeling of G3KBPY. FITC or AF750-NHS was applied to label *G3KBPY*, respectively (*SI Appendix, Materials and Methods*).

Preparation and Characterization of Nanogels. DNase I and NHS/EDC were first dissolved in ddH_2O and stirred under N_2 atmosphere for 0.5 h. G3KBPY was then added, and the mixture was dispersed for a further 12 h (*SI Appendix, Materials and Methods*).

Cell Cultures. Raw 264.7 cells were purchased from American Type Culture Collection (ATCC) and cultured in DMEM. Ramos Blue™ reporter cells were purchased from Invitrogen, and maintained in Iscove's Modified Dulbecco's Medium (IMDM). Primary RA-FLS were purchased from ATCC and grown in a DMEM/F12 medium (*SI Appendix, Materials and Methods*).

Binding Efficiency of Cationic Nanogels and cfDNA. The calf thymus DNA solution and the EtBr solution were mixed first. Different volumes of the cationic nanogels were added. After incubation at 37 °C for 24 h. The fluorescence intensity of the supernatant at a wavelength of 590 nm was measured. See *SI Appendix, Materials and Methods* for a further description of the procedures.

DNA Extraction and Measurement. For extraction of cfDNA in the plasma of mice, peripheral blood samples of RA mice were taken from the eye socket on different days and collected in EDTA-containing tubes. The cfDNA was extracted using the Dynabeads® SILANE Viral NA Kit. The concentration of cfDNA was determined with the Quanti™ PicoGreen™ dsDNA Assay Kit (*SI Appendix, Materials and Methods*).

Inhibition of TLR by Extracellular Agonists. First, 1 μM of Pam3CSK4 and 1 μM of CpG ODN 2006 were incubated with various cationic nanogels; then, the mixture was added to a 96-well plate with Ramos Blue™ reporter cells and RAW264.7 cells. After incubation for 24 h, the TLR activation, TNF-α, and IL-6 expression levels were measured using the QUANTI-Blue assay and ELISA kit, respectively (*SI Appendix, Materials and Methods*).

Western-Blotting. After the Ramos Blue™ cells were incubated with CpG 2006 in the absence or presence of cationic nanogels, cell lysates in RIPA lysis buffer were boiled and centrifuged, and the supernatant was then separated by 10% sodium dodecyl sulphate-polyacrylamide gel electrophoresis (SDS PAGE). The proteins on the PAGE were transferred to a PVDF membrane and probed with different antibodies (*SI Appendix, Materials and Methods*).

Inhibition of TLR9 by Intracellular Agonists. CpG 2006 was incubated with the Ramos Blue™ reporter cells, RAW264.7 cells and RA-FLS for 4 h in advance; then, the cationic DG3K10 nanogels at different concentrations were added. After incubation for 24 h, the TLR activation, TNF-α and IL-6 expression levels were measured using the QUANTI-Blue assay and ELISA kit, respectively (*SI Appendix, Materials and Methods*).

Cellular Colocalization of CpG and Cationic Nanogels. First, 1 μM of Quasar 670-labeled CpG 2006 with 1.0 μg/mL cationic nanogels was incubated with RAW264.7 cells for 12 h. Second, 1 μM of Quasar 670-labeled CpG 2006 was incubated with RAW264.7 cells for 4 h in advance. The excessive CpG was removed, and the cationic materials labeled with FITC (1.0 μg/mL) were added. After 4, 8, and 12 h, the cells treated in these two experiments were stained with LysoTracker Red DNA-99 and DAPI for confocal microscopic observation (Leica SP8) (*SI Appendix, Materials and Methods*).

Animal Model Induction and Treatment. The acute arthritis model was induced with CpG 2006 using 5-wk-old male Sprague−Dawley (SD) rats. Onset of arthritis occurred 1 d later, seven treatment groups (n = 5 for each group) received daily i.v. injections of PBS, MTX, G3K2, G3K5, G3K10, G2K10, and DG3K10 for 7 d. MTX (Med Chem Express®) at a dose of 2 mg/kg of body weight and cationic nanogels at a dose of 25 mg/kg of body weight were administered.

The CIA DBA-1 mice model was established by intradermal injections of bovine type II collagen with Freund's adjuvant. At 42 d postimmunization, CIA mice were randomly assigned to seven groups (n = 5 for each group) receiving i.v. injections of PBS, MTX, G3K2, G3K5, G3K10, G2K10, and DG3K10 every week (*SI Appendix, Materials and Methods*).

Biodistribution of Cationic Materials. At day 42 after immunization, the untreated CIA mice and normal mice were i.v. injected with Alexa Fluor® 750–labeled cationic nanogels. The biodistribution of the nanogels was monitored by NIRF imaging using an in vivo imaging scanner (IVIS Lumina LT, Perkin Elmer) at different time points during 24 h (*SI Appendix, Materials and Methods*).

Statistical Analysis. A one-way ANOVA test via GraphPad software (Mac version) was used to analyze experimental data wherever appropriate.

Data, Materials, and Software Availability. All study data are included in the article and/or supporting information.

ACKNOWLEDGMENTS. This work was supported by the National Key R&D Program of China (2020YFA0710800), National Natural Science Foundation of China (81930043 and T2225003), the Major International (Regional) Joint Research Project of China (grant no. 81720108020), the Natural Science Foundation of Jiangsu Province (BK20210016), and the Jiangsu Provincial Key Research and Development Program (BE2020621).

Author affiliations: [a]Department of Rheumatology and Immunology, Nanjing Drum Tower Hospital, Affiliated Hospital of Medical School, Nanjing University, Nanjing 210008, China; [b]Department of Rheumatology and Immunology, The First Affiliated Hospital of Anhui Medical University, Hefei 230022, China; and [c]State Key Laboratory of Bioelectronics, School of Biological Science and Medical Engineering, Southeast University, Nanjing 210096, China

1. O. O. Olumuyiwa-Akeredolu, M. J. Page, P. Soma, E. Pretorius, Platelets: Emerging facilitators of cellular crosstalk in rheumatoid arthritis. *Nat. Rev. Rheumatol.* **15**, 237–248 (2019).
2. M. Zheng *et al.*, Application of nanomaterials in the treatment of rheumatoid arthritis. *RSC Adv.* **11**, 7129–7137 (2021).
3. B. Peng *et al.*, Tuned cationic dendronized polymer: Molecular scavenger for rheumatoid arthritis treatment. *Angew. Chem. Int. Ed. Engl.* **58**, 4254–4258 (2019).
4. H. Liang *et al.*, Cationic nanoparticle as an inhibitor of cell-free DNA-induced inflammation. *Nat. Commun.* **9**, 4291 (2018).
5. K. Kawane *et al.*, Chronic polyarthritis caused by mammalian DNA that escapes from degradation in macrophages. *Nature* **443**, 998–1002 (2006).
6. E. Rykova *et al.*, Circulating DNA in rheumatoid arthritis: Pathological changes and association with clinically used serological markers. *Arthritis Res. Ther* **19**, 85 (2017).
7. T. Hashimoto *et al.*, Circulating cell free DNA: A marker to predict the therapeutic response for biological DMARDs in rheumatoid arthritis. *Int. J. Rheumatic Dis.* **20**, 722–730 (2017).
8. J. Wu *et al.*, Cationic block copolymer nanoparticles with tunable DNA affinity for treating rheumatoid arthritis. *Adv. Funct. Mater.* **30**, 2000391 (2020).
9. E. K. Holl *et al.*, Scavenging nucleic acid debris to combat autoimmunity and infectious disease. *Proc. Natl. Acad. Sci. U.S.A.* **113**, 9728–9733 (2016).
10. J. S. Smolen, G. Steiner, Therapeutic strategies for rheumatoid arthritis. *Nat. Rev. Drug. Discov.* **2**, 473–488 (2003).
11. J. Lee *et al.*, Nucleic acid-binding polymers as anti-inflammatory agents. *Proc. Natl. Acad. Sci. U.S.A.* **108**, 14055–14060 (2011).
12. A. B. Shodeinde *et al.*, Recent advances in smart biomaterials for the detection and treatment of autoimmune diseases. *Adv. Funct. Mater.* **30**, 1909556 (2020).
13. J. L. Kelliher, K. L. West, Q. Gong, J. W. C. Leung, Histone H2A variants alpha1-extension helix directs RNF168-mediated ubiquitination. *Nat. Commun.* **11**, 2462–2462 (2020).
14. J. Wu *et al.*, Responsive assembly of silver nanoclusters with a biofilm locally amplified bactericidal effect to enhance treatments against multi-drug-resistant bacterial infections. *ACS Cent. Sci.* **5**, 1366–1376 (2019).
15. E. C. Wayne *et al.*, Targeted delivery of siRNA lipoplexes to cancer cells using macrophage transient horizontal gene transfer. *Adv. Sci.* **6**, 1900582 (2019).
16. W. Chin *et al.*, A macromolecular approach to eradicate multidrug resistant bacterial infections while mitigating drug resistance onset. *Nat. Commun.* **9**, 917 (2018).
17. M. S. Thu *et al.*, Self-assembling nanocomplexes by combining ferumoxytol, heparin and protamine for cell tracking by magnetic resonance imaging. *Nat. Med.* **18**, 463–467 (2012).
18. H. J. Kim *et al.*, Direct conversion of human dermal fibroblasts into cardiomyocyte-like cells using CiCMC nanogels coupled with cardiac transcription factors and a nucleoside drug. *Adv. Sci.* **7**, 1901818 (2020).
19. J. Li *et al.*, Targeted combination of antioxidative and anti-inflammatory therapy of rheumatoid arthritis using multifunctional dendrimer-entrapped gold nanoparticles as a platform. *Small* **16**, e2005661 (2020).
20. S. Wu *et al.*, Poly(vinyl alcohol) hydrogels with broad-range tunable mechanical properties via the Hofmeister effect. *Adv. Mater.* **33**, e2007829 (2021).
21. Y. Ma *et al.*, Bioinspired high-power-density strong contractile hydrogel by programmable elastic recoil. *Sci. Adv.* **6**, eabd2520 (2020).
22. A. Shastri *et al.*, An aptamer-functionalized chemomechanically modulated biomolecule catch-and-release system. *Nat. Chem.* **7**, 447–454 (2015).
23. S. J. Annesley, P. R. Fisher, *Mitochondria in health and disease. Cells* **8**, 680 (2019).
24. K. M. Schmoller, J. M. Skotheim, The biosynthetic basis of cell size control. *Trends Cell Biol.* **25**, 793–802 (2015).
25. H. Zhang, K. J. Menzies, J. Auwerx, The role of mitochondria in stem cell fate and aging. *Development* **145**, dev143420 (2018).
26. W. Y. Kim, M. Won, S. Koo, X. Zhang, J. S. Kim, Mitochondrial H2Sn-mediated anti-inflammatory theranostics. *Nanomicro Lett.* **13**, 168 (2021).
27. J.-M. Heo *et al.*, A stress-responsive system for mitochondrial protein degradation. *Mol. Cell* **40**, 465–480 (2010).
28. K. Otero *et al.*, Macrophage colony-stimulating factor induces the proliferation and survival of macrophages via a pathway involving DAP12 and beta-catenin. *Nat. Immunol.* **10**, 734–743 (2009).
29. Y. Lin *et al.*, Mitochondria-inspired nanoparticles with microenvironment-adapting capacities for on-demand drug delivery after ischemic injury. *ACS Nano* **14**, 11846–11859 (2020).
30. S. H. Kim *et al.*, Reversible regulation of enzyme activity by pH-responsive encapsulation in DNA nanocages. *ACS Nano* **11**, 9352–9359 (2017).
31. J. Du, Y. S. Zhang, D. Hobson, P. Hydbring, Nanoparticles for immune system targeting. *Drug. Discov. Today* **22**, 1295–1301 (2017).
32. X. Zhang *et al.*, Engineered extracellular vesicles for cancer therapy. *Adv. Mater* **33**, e2005709 (2021).
33. Z. Zhao *et al.*, Injectable microfluidic hydrogel microspheres for cell and drug delivery. *Adv. Funct. Mater.* **31**, 2103339 (2021).
34. J. Zhao *et al.*, Dual-functional lipid polymeric hybrid pH-responsive nanoparticles decorated with cell penetrating peptide and folate for therapy against rheumatoid arthritis. *Eur. J. Pharm. Biopharm.* **130**, 39–47 (2018).
35. Y. Hu, Y. Li, F. J. Xu, Versatile functionalization of polysaccharides via polymer grafts: From design to biomedical applications. *Acc. Chem. Res.* **50**, 281–292 (2017).
36. X. Liu, S. Chen, Y. Yan, L. Liu, Y. Chen, Nanoparticulate DNA scavenger loading methotrexate targets articular inflammation to enhance rheumatoid arthritis treatment. *Biomaterials* **286**, 121594 (2022).
37. J. Dawulieti *et al.*, Treatment of severe sepsis with nanoparticulate cell-free DNA scavengers. *Sci. Adv.* **6**, eaay7148 (2020).
38. Y. Liu, X. Jiang, Why microfluidics? Merits and trends in chemical synthesis. *Lab Chip* **17**, 3960–3978 (2017).
39. H. R. Sahoo, J. G. Kralj, K. F. Jensen, Multistep continuous-flow microchemical synthesis involving multiple reactions and separations. *Angew. Chem. Int. Ed. Engl.* **46**, 5704–5708 (2007).
40. A. R. Longstreet, D. T. McQuade, Organic reaction systems: Using microcapsules and microreactors to perform chemical synthesis. *Acc Chem. Res.* **46**, 327–338 (2013).